DUAL-CIRCULARLY POLARIZED REFLECTARRAYS AS STANDARDIZED ANTENNA SOLUTIONS FOR CUBESATS

Blanca Valencia[(1)], Borja Imaz-Lueje[(2)], Daniel Martinez-de-Rioja[(1)] , Manuel Arrebola[(2)], Marcos R. Pino[(2)] , Jose A. Encinar[(1)]

[(1)]Universidad Politécnica de Madrid, Information Processing and Telecommunications Center
Madrid, Spain
Email: b.valenciag@alumnos.upm.es, jd.martinezderioja@upm.es, jose.encinar@upm.es

[(2)]Universidad de Oviedo, Department of Electrical Engineering
Gijón, Spain
Email: bimaz@uniovi.es, mpino@uniovi.es, arrebola@uniovi.es

***Abstract* – In this contribution, the design of wideband reflectarray antennas with dual linear polarization (LP) to dual circular polarization (CP) conversion is evaluated within complete operational frequency bands for space communications. The resulting antennas are proposed as standardized antenna solutions for small satellites based on the CubeSat standard, where the reflectarrays would operate in CP at the frequencies imposed by the LP radiating primary source, typically with a narrow band, while ensuring an axial ratio (AR) lower than 3 dB. Two reflectarrays have been designed: one to operate in X band, from 8 to 12 GHz, and the other to operate in Ka band, from 28 to 40 GHz. The manufacturing of broadband LP-to-CP reflectarrays could be carried out in a production line, reducing the costs and complexity of ad-hoc reflectarrays, while also simplifying the design of the LP feeds.**

I. INTRODUCTION

The increasing number of space missions based on small satellites, especially CubeSats [1], has driven the development of novel high-gain antennas to be deployed on the small satellites. The use of high-gain antennas plays a key role in transmitting and receiving signals over longer distances and increasing the link capacity to send a larger volume of data in a short period of time. Additionally, in satellite communications, the operation in circular polarization (CP) is preferred over linear polarization (LP) for its enhanced reliability, as it minimizes signal fading caused by changes in the satellite orientation and the Faraday effect as signals pass through the Earth atmosphere.

The CubeSat platform implies two additional antenna requirements: the antenna should occupy the least amount of space possible, given the constrained storage volume of CubeSats, and it should also be cost-effective, aligning with the principle of offering low-cost satellite missions. The small stowage volume of CubeSats makes it difficult to embark traditional high-gain antennas, such as reflectors antennas, whose doubly curved surface is difficult to fold.

Reflectarray antennas offer a promising high-gain antenna solution for small satellites [2]-[6], since their flat surface can be easily divided into multiple flat panels that can be folded around the spacecraft before the launching, and then deployed through the same technology standardized for solar panels. The use of deployable multi-panel reflectarrays for CubeSat missions has been recently demonstrated in the ISARA and MarCO missions [2], [3], and are also expected to be used in the GOMX-5 and M-ARGO missions [5], [6]. As an additional advantage for small satellite scenarios, reflectarray antennas can be designed to convert the incident LP field radiated by a primary source into a reflected CP field, thus simplifying the design and architecture of the primary source on board the satellite [7], [8]. However, reflectarray antennas have two major concerns on their deployment for industry: their natural narrowband performance, which may be further reduced when providing an additional LP-to-CP polarization conversion, and the necessity of a customized optimization and manufacturing of the antenna for the specific frequency band of each application, which increases the antenna manufacturing costs and development times.

In this contribution, the design of wideband reflectarray antennas with dual-LP to dual-CP conversion is evaluated with the aim of providing an axial ratio below 3 dB within a complete operational frequency band for space. For this purpose, two polarizer reflectarrays are designed: one to operate in X band, from 8 to 12 GHz, with a maximum gain over 24 dB, and the other to operate in Ka band, from 28 to 40 GHz, with a maximum gain over 30 dBi. The proposed antennas could work as standardized antenna solutions for small satellites based on the CubeSat standard, where the reflectarray would operate in CP at the frequencies imposed by the LP radiating primary source, typically with a narrow band, while ensuring a satisfactory polarization purity. The designed reflectarrays can be fabricated by dividing the antenna surface into several panels, making it easy to

fold around the CubeSat [2]. As a result, the production of broadband multi-faceted reflectarrays could be efficiently carried out in a production line, reducing the costs and complexity associated with ad-hoc reflectarrays, while also simplifying the design of the LP feeds.

II. Antenna Configuration

CubeSat standard defines the fundamental element of the spacecraft as a cube of 10 cm × 10 cm × 10 cm, known as 1U. These cubes can be easily stacked and integrated into larger payloads. As shown in Fig. 1, the most extended spacecrafts consist of one (1U), two (2U) three (3U), six (6U) or twelve (12U) elemental cubes. The standardization of the spacecraft architecture made it possible to streamline the manufacturing process, helping to ensure compatibility of components and design specifications while ~~reducing significantly~~significantly reducing the associated costs and development times.

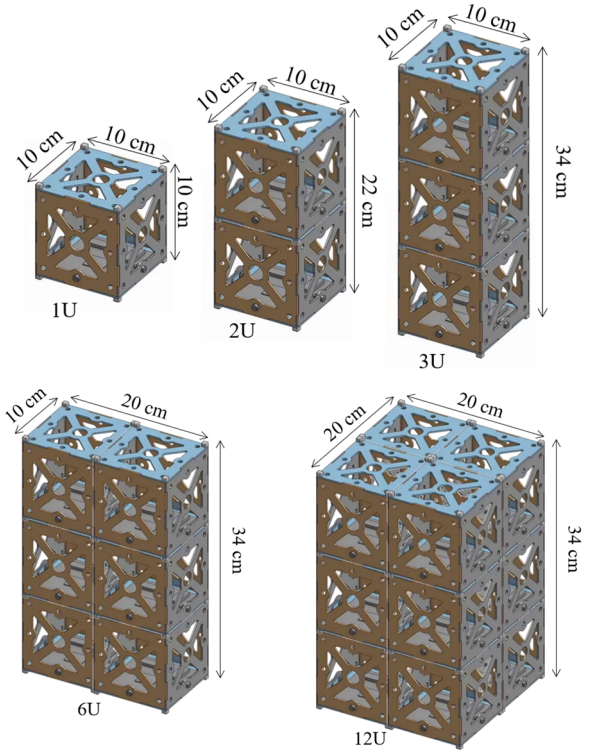

Fig. 1. Basic architecture of 1U, 2U, 3U, 6U and 12U CubeSats.

The design of high-gain reflectarray antennas as standard antenna solutions for CubeSat applications must take into consideration the available volume in the spacecraft to accommodate the reflectarray and its primary source of radiation, which is considered as a planar small printed LP array. Due to the narrow beam produced by the high-gain antennas, the CubeSat should also incorporate a high-precision altitude control subsystem for a proper antenna pointing. Given these requirements, CubeSats smaller than 3U have not been considered when defining the antenna architecture. It is worth noting that ~~MarCo~~ MarCO and ISARA missions [2], [3] employed 12U and 3U CubeSats to embark high-gain reflectarrays, and GOMX-5 and M-ARGO missions [5], [6] also consider 12U CubeSats.

Fig. 2 illustrates the proposed antenna architecture for both the stowed configuration around the spacecraft and its deployment once in orbit. Since the panels must be deployed forming a flat surface, dividing the reflectarray antenna into several panels can be seen as a mechanical consideration, independent of the electrical design of the reflectarray antenna. Also, note that the stowed reflectarray could be folded above the feed, due to the low profile of both antennas. As a result, the reflectarray antenna can be defined with an approximate dimension of 30 cm × 30 cm for the 3U CubeSat, consisting of three panels of 10 cm × 30 cm, or 20 cm × 20-30 cm for the single-panel reflectarray proposed for 6U/12U CubeSats. The decision to use a multi-panel configuration for the reflectarray can also be adopted for 6U/12U CubeSats if a larger antenna aperture is required. In both configurations, the feed must be positioned at a distance equal to or less than the length of the spacecraft (see spacecraft dimensions in Fig. 1), keeping the simplicity of the deployment mechanism for both the reflectarray and the feed.

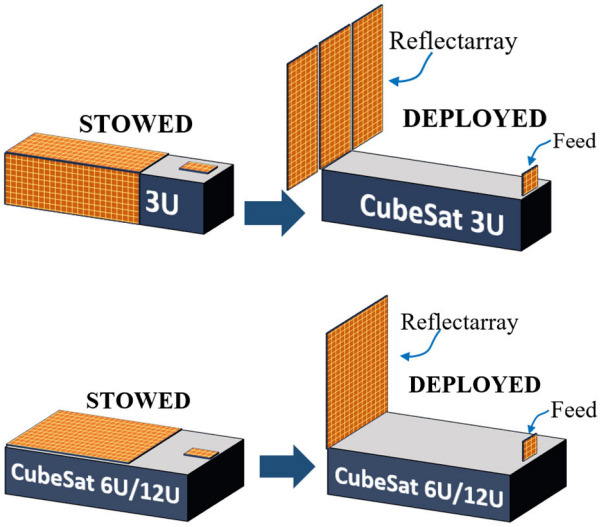

Fig. 2. Schematic representation of the antenna configuration on 3U and 6/12U CubeSat platforms.

Two reflectarray antennas (RA) have been proposed according to these scenarios. A reflectarray antenna to operate in X-band (X-RA) and a reflectarray to operate in Ka-band (Ka-RA). The X-RA is a 280.5 mm × 280.5 mm ($8\lambda_0$ × $8\lambda_0$ at 8.5 GHz), formed by 17 × 17

reflectarray cells with a period of 16.5 mm ($0.48\lambda_0$ at 8.5 GHz). The phase centre of the feed is positioned at coordinates (x = -115.6, y = 0.0, z = 247.8) mm with respect to the centre of the reflectarray, giving a focal length to diameter ratio (f/D) of 1. The Ka-RA is a 202.4 mm × 202.4 mm ($21\lambda_0 \times 21\lambda_0$ at 31 GHz), formed by 44 × 44 cells of 4.6 mm ($0.48\lambda_0$ at 31 GHz). The Ka-RA is illuminated by a feed placed at (x = -78, y = 0.0, z = 180.1) mm with respect to the antenna centre, resulting in a f/D of 0.8. The use of a f/D larger than 1 would improve the antenna bandwidth by minimizing the differential spatial phase delay [9], but it also requires high-gain feeds to properly illuminate the reflectarray with a taper close to -10 dB at the edges, which increases the size of the primary sources. The X-RA radiates in the direction $\theta_b = 19º$, $\varphi_b = 0º$, while the Ka-RA radiates in $\theta_b = 23º$, $\varphi_b = 0º$. Table 1 summarizes the main characteristics of the proposed antenna configurations.

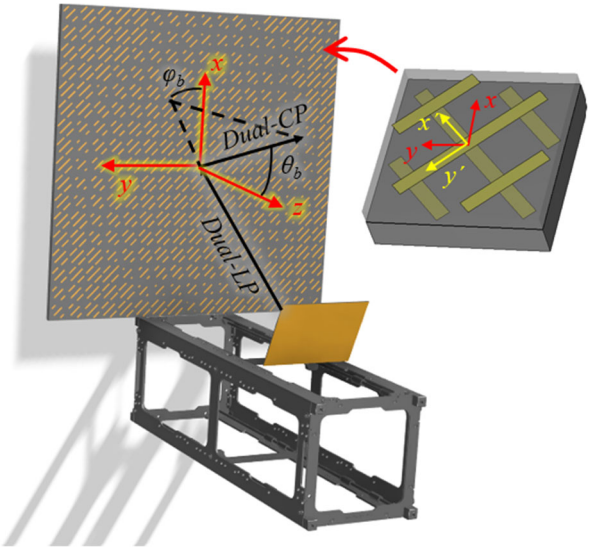

Fig. 3. Antenna configuration for the X-RA.

Table 1. Proposed antenna configurations.

Prototype	**X-RA**	**Ka-RA**
Polarization	Dual-CP	Dual-CP
Frequency band	8-12 GHz (40%)	28-40 GHz (35%)
Antenna size	$8\lambda_0 \times 8\lambda_0$ at 8.5 GHz (280.5 mm)	$21\lambda_0 \times 21\lambda_0$ at 31 GHz (202.4 mm)
f/D	1	0.8
Beam direction (θ_b, φ_b)	(19º, 0º)	(23º, 0º)
Cell period	$0.48\lambda_0$ at 8.5 GHz (16.5 mm)	$0.48\lambda_0$ at 31 GHz (4.6 mm)
Cell lattice	17 × 17	44 × 44

III. Reflectarray Unit-Cell

The proposed reflectarray antennas have a dual-layer configuration with two levels of metallization. The unit-cell consists of two stacked orthogonal groups of three parallel dipoles, which are rotated 45º with respect to the antenna axes, as shown in Fig. 3 for the X-RA. Fig. 4 illustrates the proposed unit-cell including the main geometrical parameters. The unit-cells have been defined with the same period of $0.48\lambda_0$ at the design frequency of each antenna (8.5 GHz for the X-RA and 31 GHz for the Ka-RA). For their future experimental validation, both antennas have been designed considering DiClad 880 substrates (ε_r = 2.28, tanδ = 0.0025). The Ka-RA uses two identical sheets of 0.762 mm DiClad 880, while the X-RA employs a lower sheet of 3.175 mm DiClad 880 and a thinner upper sheet of 1.524 mm DiClad 880. The period of the cells (p_X, p_Y), the separation between adjacent dipoles (s) and the dipoles width (w) are shown in Table II for both prototypes. The geometrical parameters of the cells are practically scaled from one prototype to another, except for small differences produced by the different dielectric configurations. The lengths of the upper and lower dipoles (l_{A2}, l_{A1}, l_{B2}, l_{B1}) will be adjusted cell by cell during the design process of the antenna.

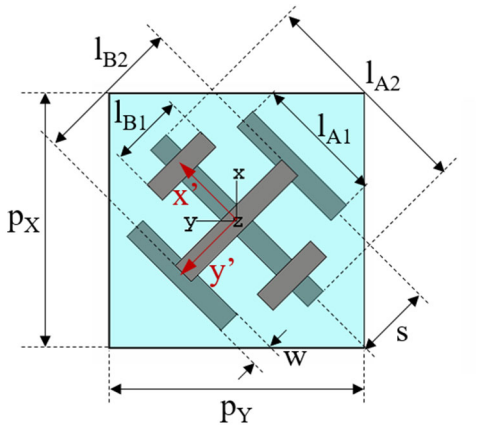

Fig. 4. Antenna configuration for the X-RA.

Table 2. Cell configurations.

Prototype	**X-RA**	**Ka-RA**
p_X (= p_Y)	16.5 mm	4.6 mm
s	6 mm	1.4 mm
w	1.4 mm	0.4 mm
Lower dielectric height	3.175 mm (125 mils)	0.762 mm (30 mils)
Upper dielectric height	1.524 mm (60 mils)	0.762 mm (30 mils)

The unit-cell has been defined to convert the dual-LP incident field into a dual-CP reflected field, while focusing a high gain beam. The lengths of the upper and

lower dipoles are independently adjusted to control the phase-shift introduced in the orthogonal linear components of the reflected field oriented according to x' and y' (see Fig. 3 and 4). Thus, the reflectarray cell can be analysed by its reflection matrix in the (x', y') coordinate system, as shown in (1). The 45º rotation of the dipoles is necessary to provide the conversion from dual LP to dual CP [7], [8]. The polarization conversion is provided when there is a 90º phase difference between the phases of R'_{XX} and R'_{YY} ($\angle R'_{XX} - \angle R'_{YY} = 90º$).

$$\begin{pmatrix} E^r_{x'} \\ E^r_{x'} \end{pmatrix} = \mathbf{R'_{XY}} \begin{pmatrix} E^i_{x'} \\ E^i_{y'} \end{pmatrix} = \begin{pmatrix} R'_{XX} & R'_{XY} \\ R'_{YX} & R'_{YY} \end{pmatrix} \cdot \begin{pmatrix} E^i_{x'} \\ E^i_{y'} \end{pmatrix} \quad (1)$$

The reflectarray cells have been analysed using a proprietary software based on the method of moments in the spectral domain (SD-MoM) [7], which assumes local periodicity to analyse the cell under any angle of incidence by calculating its reflection matrix $\mathbf{R'_{XY}}$. This home-made analysis routine has been previously validated by commercial software tools and experimental demonstrators. The phase performance of the cells has been simulated when the upper and lower dipoles are independently increased, considering that the lengths of the lateral dipoles in each set of three parallel dipoles remain scaled by a fixed factor with regards to the length of the central dipoles. For the X-RA cell, the lengths of the lateral dipoles are defined as $l_{A1} = 0.45 \cdot l_{A2}$, and $l_{B1} = 0.55 \cdot l_{B2}$, while the lengths of the lateral dipoles in the Ka-RA cell are defined as $l_{A1} = 0.59 \cdot l_{A2}$, and $l_{B1} = 0.5 \cdot l_{B2}$ (see Fig. 4). The cells have been analysed under an incidence angle $\theta_i = 20º$, $\varphi_i = 0º$, which matches the incidence angle at the antenna centre in both prototypes.

The simulated phase response of the X-RA cell at 8.5 GHz is depicted in Fig. 5, including the phases of R'_{XX} (Fig. 5(a)), R'_{YY} (Fig. 5(b)), and its difference $\angle R'_{XX} - \angle R'_{YY}$ (Fig. 5(c)) when the upper and lower dipoles lengths vary from 8 mm to 19.5 mm. The phases of R'_{XX} and R'_{YY} have a phase range larger than 360º and show an independent operation (the lengths of the lower dipoles, given by l_{A2}, control the phase of R'_{XX}, and the lengths of the upper dipoles, given by l_{B2}, control $\angle R'_{YY}$). Moreover, Fig. 5(c) includes a solid black line indicating the combinations of dipole lengths that provide a 90º phase difference between $\angle R'_{XX}$ and $\angle R'_{YY}$, necessary for the LP to CP polarization conversion. It is important to note that the black line spans a phase shift region larger than 360º in both $\angle R'_{XX}$ and $\angle R'_{YY}$, thus ensuring the capability of converting the dual-LP incident field intro a dual-CP reflected field while simultaneously introducing a phase distribution to focus a high-gain beam. The same phase response can be seen in Fig. 6 for the Ka-RA cell at 31 GHz.

IV. Antenna Design

The phase-shift distributions for $\angle R'_{XX}$ and $\angle R'_{YY}$ on the reflectarray surface have been computed to focus a ~~high~~ high-gain beam in the direction ($\theta_b = 23º$, $\varphi_b = 0º$) at 8.5 GHz for the X-RA prototype, and ($\theta_b = 19º$, $\varphi_b = 0º$) at 31 GHz in the Ka-RA. The reflectarray theory [10] defines the required phase-shift distribution to focus a ~~high~~ high-gain beam by (2), where ϕ_{R-i} is the required phase-shift introduced by the cell i, placed at coordinates x_i, y_i with respect to the reflectarray centre, d_i is the distance between the centre of the cell i and the phase centre of the feed, and (θ_b, φ_b) is the direction of radiation. The term $\Delta\phi$ is a phase constant that makes it possible to introduce the required 90º phase difference between the phase-shift distributions of $\angle R'_{XX}$ and $\angle R'_{YY}$ to convert the polarization while also focusing a high-gain beam. Fig. 7 shows the required phase distributions of $\angle R'_{XX}$ for both prototypes, the phases of $\angle R'_{YY}$ can be obtained by adding a 90º phase constant to the distributions shown in Fig. 7.

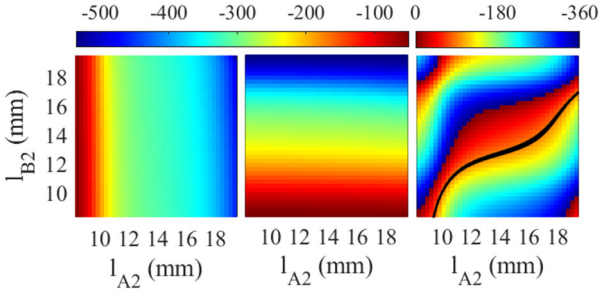

(a) (b) (c)

Fig. 5. Phase (º) introduced by the X-RA cell at 8.5 GHz versus the dipoles lengths. (a) $\angle R'_{XX}$, (b) $\angle R'_{YY}$', and (c) $\angle R'_{XX} - \angle R'_{YY}$.

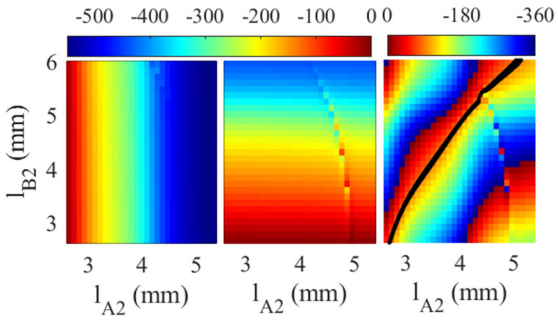

(a) (b) (c)

Fig. 6. Phase (º) introduced by the Ka-RA cell at 31 GHz versus the dipoles lengths. (a) $\angle R'_{XX}$, (b) $\angle R'_{YY}$', and (c) $\angle R'_{XX} - \angle R'_{YY}$.

The design process has been carried out by an optimization routine based on the previous SD-MoM analysis tool, which adjusts the lengths of the dipoles, cell by cell, taking into account the different angles of incidence in each cell along the antenna surface. To overcome the limited bandwidth of reflectarray antennas, which is even reduced when providing an

additional LP-to-CP polarization conversion, an optimization process has been implemented thanks to the degrees of freedom provided by the proposed cell. The cell offers two design variables to control the phases of each linear component of the reflected field (l_{A2} and l_{A1} to control R'_{XX}, and l_{B2} and l_{B1} to control R'_{YY}). The optimization process has been implemented to minimize the phase errors with respect to the objective phases at the design frequency (f_0 = 8.5 GHz for the X-RA and f_0 = 31 GHz for the Ka-RA) computed by (2), while also minimizing the phase deviation with regards to the required 90º phase difference between $\angle R'_{XX}$ and $\angle R'_{YY}$ at two extreme frequencies (f_{min}, f_{max}). Note that f_0 is defined relatively close to the minimum frequency of the band with the aim of maximizing the antenna efficiency at low frequencies. In this way, as the operating frequency increases, the antenna efficiency decreases but the larger electrical size of the reflectarray keeps the maximum gain of the antenna stable within the band.

$$\phi_{R-i} = k_0(d_i - (x_i\cos\varphi_b + y_i\sin\varphi_b)\sin\theta_b) + \Delta\phi \quad (2)$$

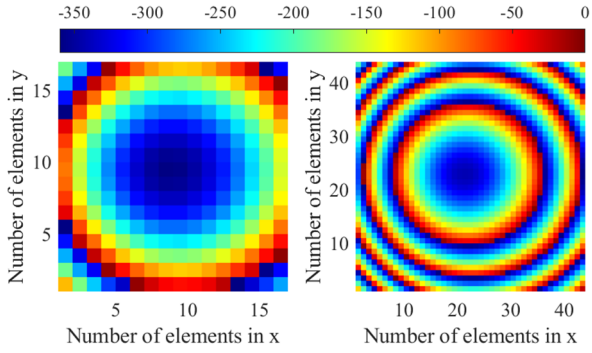

(a) (b)

Fig. 7. Required phases of $\angle R'_{XX}$ (º) (a) at 8.5 GHz for the X-RA, and (b) at 31 GHz for the Ka-RA.

V. Simulated Results

The simulated radiation patterns of the designed reflectarrays have been computed from the tangential components of the reflected field on the reflectarray surface, computed as shown in (1). Two horns (Narda640-15 for the X-RA and Narda665-20 for the Ka-RA) have been considered to illuminate the reflectarrays, making it possible to evaluate the radiation patterns in the complete X and Ka band. The feed-horns have been modelled in CST to compute the incident field on the reflectarray surface.

The elevation cut of the simulated radiation patterns for the X-RA at 8.5 GHz and for the Ka-RA at 31 GHz are shown in Fig. 8 and Fig. 9. The X-RA and the Ka-RA show a maximum gain of 25.5 and 33 dBi, respectively, which corresponds to a radiation efficiency of 43% in both antennas. Also, the cross-polar discrimination (XPD) is larger than 20 dB in both reflectarrays, providing an axial ratio (AR) lower than 3dB.

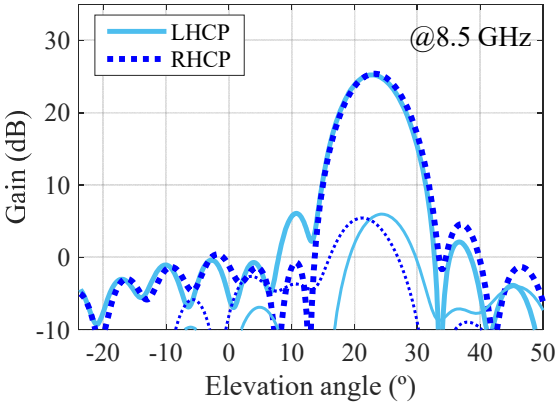

Fig. 8. Elevation plane of the X-RA simulated radiation patterns at 8.5 GHz.

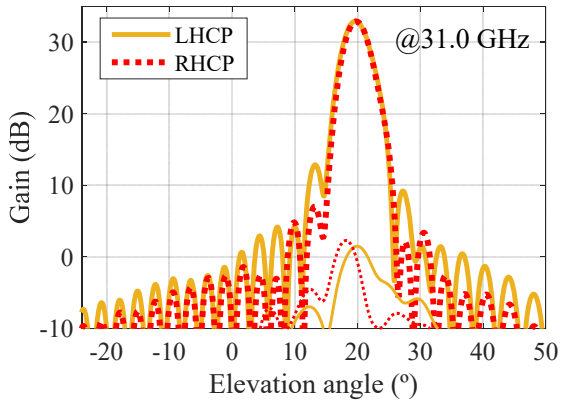

Fig. 9. Elevation plane of the Ka-RA simulated radiation patterns at 31 GHz.

The simulated radiation patterns of the X-RA have been computed from 7 to 14 GHz. The curves of maximum gain and AR provided by the X-RA are depicted in Fig. 10. The simulated results show that the reflectarray antenna can operate from 8 to 12 GHz ensuring a maximum gain comprised between 24.3 to 25.5 dBi. The 3dB-bandwidth in gain is reached from 7.5 to 13.5 GHz, where the AR is lower than 3 dB. Thus, the linear-to-circular polarizer X-RA offers a 57% relative bandwidth (RBW) instead of the 10% RBW typically provided by non-optimized polarizer reflectarrays [7]. The simulated gain and AR for the Ka-RA are shown in Fig. 11 from 27 to 42 GHz. The Ka-RA has a maximum gain over 30 dBi from 28 to 40 GHz, varying from 30.1 to 33.7 dBi, while providing an AR lower than 3 dB. The Ka-RA provides a slightly smaller RBW than the X-RA (a 35% RBW), which makes it possible to enhance the polarization purity within the complete band: the AR is lower than 1.5 dB from 28.75 to 41.25 GHz.

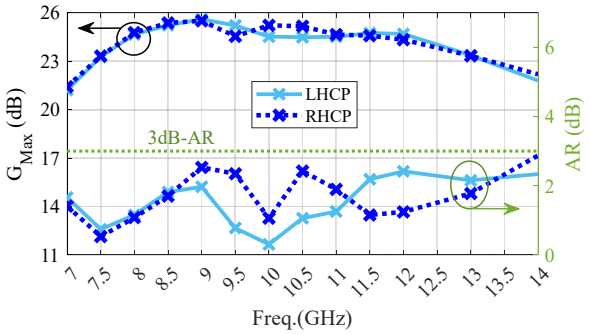

Fig. 10. Maximum gain and AR of the X-RA.

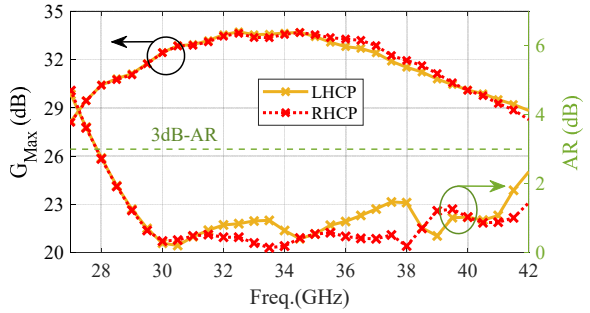

Fig. 11. Maximum gain and AR of the Ka-RA.

These antennas could work as standardized antenna solutions operating in a narrow band imposed by the LP feed within the X-band or Ka-band. Note that the maximum gain of the antennas may vary slightly depending on the taper provided by the feed at the reflectarray edges.

VI. Conclusions

In this contribution, the design of wideband reflectarray antennas with dual-LP to dual-CP conversion has been evaluated as standardized antenna solutions for CubeSats. Two reflectarrays have been designed, one to operate from 8 to 12 GHz, and the other to operate from 28 to 40 GHz, providing an axial ratio lower than 3 dB in both cases. The proposed reflectarrays could be manufactured in a production line to operate at narrow frequency bands imposed by the feed-chain according to the specifications of each mission. The polarization conversion makes it possible to operate in CP by using a LP feed, which also simplifies the design of the feed-chain. This concept can be extended to other frequency bands of interest.

Acknowledgements

This work was supported in part by MICIN/AEI/10.13039/501100011033 within the projects PDC2021-120959-C21, TED2021-130650B-C22, by the Spanish Ministry of Universities (RD 289/2021, UP2021-035), funded by the NextGenerationEU under the Recovery plan for Europe and by Gobierno del Principado de Asturias under project AYUD/2021/51706 and by Spanish Ministry of Education under grant FPU18/0575.

VII. References

[1] J. Puig-Suari, C. Turner and W. Ahlgren, "Development of the standard CubeSat deployer and a CubeSat class PicoSatellite," *2001 IEEE Aerospace Conference Proceedings*, Big Sky, MT, USA, 2001, pp. 1/347-1/353.

[2] R. E. Hodges, M. J. Radway, A. Toorian, D. J. Hoppe, B. Shah and A. E. Kalman, "ISARA - Integrated Solar Array and Reflectarray CubeSat deployable Ka-band antenna," *2015 IEEE International Symposium on Antennas and Propagation (APS-URSI)*, Vancouver, BC, Canada, 2015, pp. 2141-2142.

[3] R. E. Hodges, N. Chahat, D. J. Hoppe and J. D. Vacchione, "A Deployable High-Gain Antenna Bound for Mars: Developing a new folded-panel reflectarray for the first CubeSat mission to Mars," *IEEE Antennas and Propagation Magazine*, vol. 59, no. 2, pp. 39-49, April 2017.

[4] N. Chahat, E. Thiel, J. Sauder, M. Arya and T. Cwik, "Deployable One-Meter Reflectarray For 6U-Class CubeSats," *2019 13th European Conference on Antennas and Propagation (EuCAP)*, Krakow, Poland, 2019, pp. 1-4.

[5] "GOMX-5 (GomSpace Express-5)", eoPortal, https://www.eoportal.org/satellite-missions/gomx-5#mission-capabilities. Accessed: 09/08/2023.

[6] "M-Argo: Journey of a suitcase-sized asteroid explorer", European Space Agency – ESA, https://www.esa.int/Enabling_Support/Space_Engineering_Technology/Shaping_the_Future/M-Argo_Journey_of_a_suitcase-sized_asteroid_explorer. Accessed: 09/08/2023.

[7] D. Martinez-de-Rioja, B. Imaz-Lueje, J. A. Encinar, M. Arrebola and M. R. Pino, "Dual Circularly Polarized Reflectarray Antenna for High Throughput Links from Small Satellites," *2023 17th European Conference on Antennas and Propagation (EuCAP)*, Florence, Italy, 2023, pp. 1-4.

[8] E. Martinez-de-Rioja, I. Linares and D. Martinez-de-Rioja, "Dual-Band Polarizer Reflectarray Operating in Dual-CP for High-Gain Antenna in CubeSats," *2022 16th European Conference on Antennas and Propagation (EuCAP)*, Madrid, Spain, 2022, pp. 1-5.

[9] John Huang, Jose A. Encinar, "Broadband Techniques" in *Reflectarray Antennas*, IEEE, 2008, pp.93-118..

[10] John Huang, Jose A. Encinar, "Antenna Analysis Techniques" in *Reflectarray Antennas*, IEEE, 2008, pp.27-35, doi: 10.1002/9780470178775.ch3.